Slip sequences in laboratory experiments as analogues to earthquakes associated with a fault edge

Shmuel M. Rubinstein, Gil Cohen , & Jay Fineberg
The Racah Institute of Physics, The Hebrew University of Jerusalem, Givat Ram, Jerusalem 91904, Israel

Ze'ev Reches
School of Geology and Geophysics, University of Oklahoma, Norman, 73019, OK

ABSTRACT: Natural faults are intrinsically heterogeneous where jogs, edges and steps are common. We experimentally explore how fault edges may affect earthquake and slip dynamics by applying shear to the edge of one of two flat blocks in frictional contact. We show that slip occurs via a sequence of rapid rupture events that arrest after a finite distance. Successive events extend the slip size, transfer the applied shear across the block, and cause progressively larger changes of the contact area along the contact surface. Each sequence of events dynamically forms an asperity near the edge and largely reduces the contact area beyond. These sequences of rapid events all culminate in slow slip events that lead to major, unarrested slip along the entire contact surface. These results show that a simple deviation from uniform shear loading configuration can significantly and qualitatively affect both earthquake nucleation processes and the evolution of fault complexity.

1 INTRODUCTION

Faults are often modelled as planar interfaces separating two elastic half-spaces that are driven by a spatially uniform shear that is imposed by the motion of tectonic plates[*Das*, 2003; *Lapusta and Rice*, 2003; *Rice and Ben-Zion*, 1996] On the other hand, the loading of a natural fault is the superposition of the uniform shear due to remote loading (e.g., plate motion), and nonuniform loading generated by local structural features. Heterogeneities (e.g. steps, jogs, asperities and edges) [*Ben-Zion and Sammis*, 2003; *Harris and Day*, 1993; *Shaw and Dieterich*, 2007; *Wesnousky*, 2006], abound within the seismogenic zone. This complexity may govern some of the dominant properties of earthquakes.

In this paper we experimentally explore the influence of one type of nonuniformity: loading on the edge of a fault which, initially, is smooth and uniform. Our laboratory "fault" is formed by two elastic blocks separated by a roughened, but optically flat, frictional interface. Shear force is applied to one edge of the slider block (Figure 1a) while a uniform normal stress is remotely applied. This loading configuration is a simplified model for the inhomogeneous loading that is likely to occur at an edge or asperity along an otherwise planar fault. In order to highlight the unique contributions of the nonuniform application of shear to the resulting fault dynamics, this model focuses on the effects of the nonuniform component and ignores the uniform component of the applied shear.

We believe that similar effects such as those described in the paper occur in-situ, due the common presence of structural perturbations within natural faults. Configurations in which edge-loading may play an important role are common along active faults in the earth's crust, and include: slip along a segment within a long fault that loads the neighbouring segments at the edge of the slipped region (e.g. north Anatolian fault [*Stein et al.*, 1997], the physical edges formed between abutting segments (e.g. the intersection of the Susitna Glacier and Denalli

faults [*Aagaard and Heaton*, 2004], and by asperities and steps along faults [*Harris and Day*, 1993; *Johnson et al.*, 1994 ; *Lay et al.*, 1982; *Sagy et al.*, 2007; *Shaw and Dieterich*, 2007; *Wesnousky*, 2006]. As these examples show, the loading of large crustal faults is frequently modelled by a combination of "basal loading" on the crust base, and "edge loading" at the fault edge [*Lachenbruch and Sass*, 1980; *Matsuura and Sato*, 1997; *Reches et al.*, 1994].

2 EXPERIMENTAL METHODS

The experimental setup used is described in detail in [*Rubinstein et al.*, 2004; *Rubinstein et al.*, 2006]. We performed real-time measurements of the *true* area of contact, *A(x,y,t)*, along the entire interface separating two polymethyl-methacrylate blocks whose (*x*:*y*:*z*) dimensions were 300:30:27*mm* for the static ("base") block and either 140:6:75*mm* or 200:6:75*mm* for sliding ("slider") block. *x*, *y*, and *z* are, respectively, the sliding, sample width, and normal loading directions. The optically flat base-slider interface was roughened to 1μm rms. For the range ($1 < F_N < 4$ kN) of normal load, (F_N), applied, *A(x,y,t)* varied from 0.35 -1.35 % of the interface's nominal contact area [*Dieterich and Kilgore*, 1994]. *A(x,y,t)* was measured by illuminating the contact area by a laser sheet whose incident angle was well beyond the angle for total internal reflection from the interface. Thus light is transmitted only at points of contact, with an intensity at each point (*x*,*y*) proportional to *A(x,y,t)*. *A(x,y,t)* was imaged at rates up to 100,000 frames/sec. The data acquisition was designed to capture both slow processes at the quasi-static time scales governed by the loading rate and rapid, crack-like, processes whose entire duration takes place in the sub-msec range. As the onset dynamics are governed by one-dimensional rupture fronts [*Rubinstein et al.*, 2004], *A(x,y,t)* was averaged in *y*, yielding *A(x,t)* to 1280 pixel resolution. Thus, *A(x,t)* yields a local measurement of the contact area, where each pixel measures the integrated contact area a 0.1mm × 6mm region (with the higher resolution in the direction of motion). At the initiation of each experiment, before the application of shear the slider was oriented relative to the base to form an initial contact area that was, statistically, spatially uniform (utilizing the *A(x,y)* measurements to guide the positioning). Upon completion of this initial positioning, F_N was applied. The corresponding value of *A(x,t=0)* was then used to normalize subsequent measurements of *A(x,t)* to allow us to measure the changes in *A(x,t)* resulting from the dynamics at each point *x*.

At *t=0*, the shear force, F_S, was applied in the *x* direction to one edge (the ''trailing'' edge at *x*=0) of the slider at a height *z*=*h* ($2 < h < 18$ *mm*) above the interface (see Figure 1a). F_S was increased from zero at constant rates (range 1-20 μm/s) until, at $F_S=\mu_S F_N$, stick-slip sliding initiated. The precise means by which F_S was applied was unimportant (e.g. via rigid blocks of various dimensions), as long as *h* was defined as the mean height of the applied shear force. In this loading system [*Rubinstein et al.*, 2006], any slip of the trailing edge immediately results in a sharp drop of F_S. While the leading edge (at *x*=*L*) is stationary, drops of F_S mirror the stress release across the interface.

3 RESULTS

3.1 *Slip sequences and stress history*

Concurrent measurements of contact area *A(x,t)*, and shear load $F_S(t)$ for a typical experiment (Figure 1b) reveal that large stick-slip events are the culmination of a complex history of precursory slip events. The $F_S(t)$ curve in Figure 1b reveals a discrete sequence of small sharp stress drops that occur at stress levels well below the peak values of $F_S(t)$. These small stress drops (of ~ $0.01\text{-}0.02 \cdot F_S$) result from the propagation of a sequence of rapid, crack-like arrested slip events. The measurements of *A(x,t)* at short times (Figure 2a - top) show that the initial slip events begin at the trailing edge, and propagate at "sub-Rayleigh" speeds, typically between 60%-80% of the Rayleigh wave speed (V_R), before abruptly arresting (Figure 2b). These initial events (Figure 2a – top) are associated with slipping segments of length *l* that are relatively small compared to the entire fault size, *L*. We find that *l* obeys a linear scaling relation

[*Rubinstein et al.*, 2007], $l \propto F_S\, L/F_N$ (Figure 3a). Once l approaches 0.4-0.5L, this scaling breaks down and the initial dynamics undergo a qualitative change that marks a transition [*Rubinstein et al.*, 2004; *Rubinstein et al.*, 2006] into a new stage. The slip events in this stage also initiate at the trailing edge as rapid sub-Rayleigh slip events, but do not simply arrest. Instead, these larger events trigger a "slow" front that propagates at speeds over an order of magnitude slower (~ 50*m/sec* in Figure 2b) than the sub-Rayleigh velocities of the triggering events. These slow fronts can propagate stably for some time, and either traverse the remainder of the interface or transition back to sub-Rayleigh fronts, as shown in Figure 2a (bottom). Significantly, overall motion (sliding) between the blocks initiates only after either a slow or subsequently triggered sub-Rayleigh front has reached the leading edge.

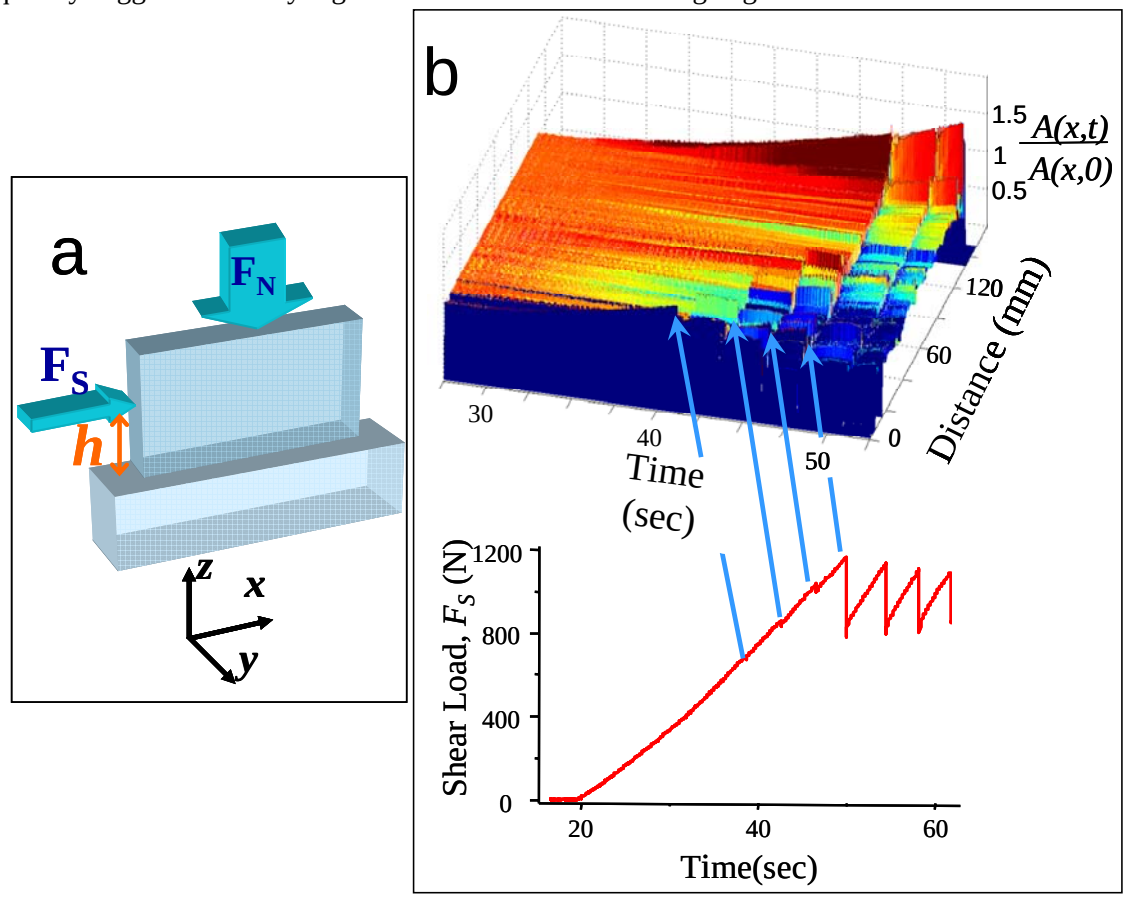

Figure 1: The transition to stick-slip sliding is preceded by a sequence of discrete arrested slip events. **a,** A schematic illustration of the base and slider blocks and load application **b,** (bottom) Applied shear force, F_S, as a function of time with the (top) corresponding spatio-temporal evolution of A(x,t). Each small discrete drop in F_S corresponds to a rapid slip event that arrests within the interface. Each arrested slip event generates significant changes in A(x,t). Arrested events, together with the corresponding drop in shear load, are denoted by the arrows. The large stress drops mark stick-slip motion. Interface length, L=140mm, F_N=3.3 kN.

The discrete sequence of such arrested slip events, described by Figure 1, is *only* observed when shear is imposed at the sample's trailing edge. It is not observed when, for example, a uniform shear stress is imposed at a remote boundary parallel to the interface. With the trailing edge loading, each sequence initiates via a slip event of finite length, l_0, with l increasing by discrete increments, Δl, of constant length for each successive slip.

Figure 3b shows that the size of both l_0 and Δl is proportional to h, the height above the interface where F_S is applied at the edge. Note that h, however, has no effect on the overall scaling of l (Figure 3a). Since l scales linearly with F_S, the fixed value of Δl (for a given h) indicates that slip events occur at fixed intervals, ΔF_S, in F_S. Thus, h, which determines Δl, governs also the magnitude of the intervals, ΔF_S, between successive events. For a constant shear loading rate, (as in our experiments) the temporal periods between events are proportional to h.

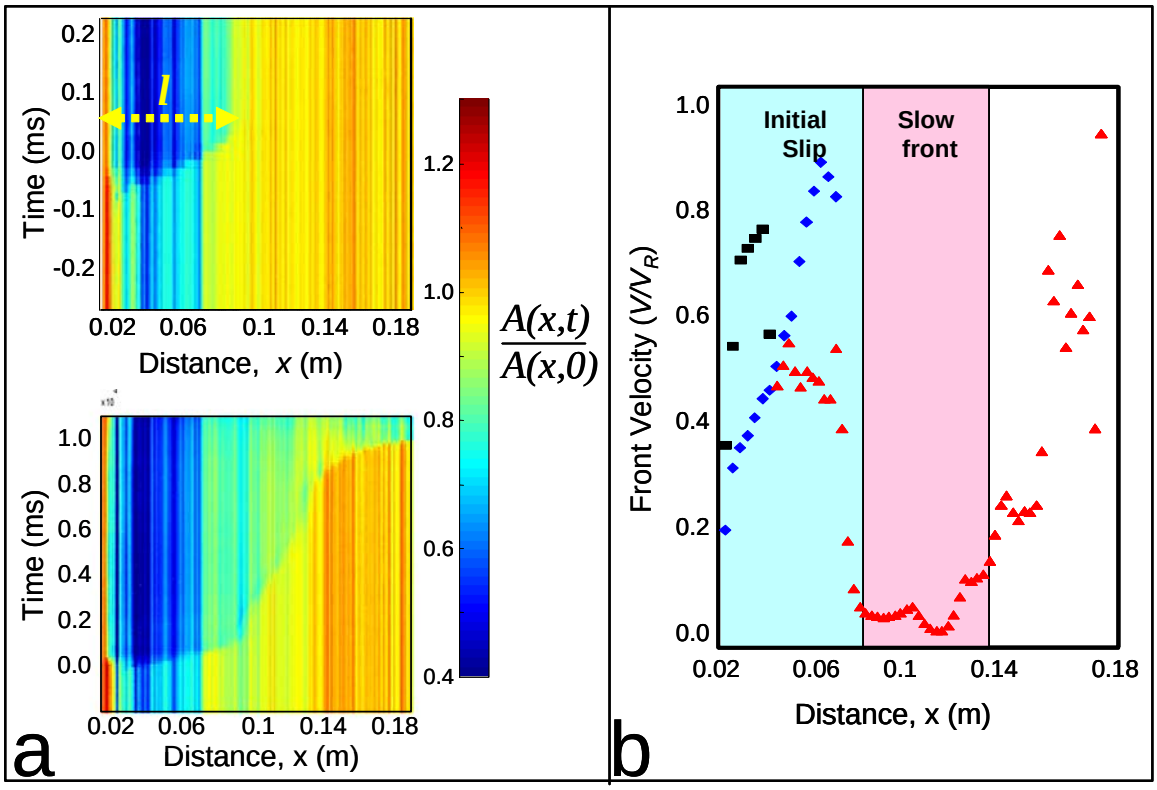

Figure 2: **a,** (top) An arrested slip event of length, *l*, generated at stresses well below the onset of stick-slip. (bottom) The transition to stick-slip motion at the peak value of F_S. Here rapid slip arrests and triggers a slow front. At x=0.14m the slow front nucleates a rapid slip that traverses the remainder of the interface. Color bar indicates the change in $A(x,t,)$, relative to the initial, uniform value $A(x,t=0,)$ when F_S=0. $A(x,t)$, measured at 14μsec intervals in two different events. **b,** The slip propagation velocities (as a function of x) of arrested events (diamonds and squares) and the transition (triangles) to stick-slip motion. Events depicted by diamonds and triangles correspond to (a).

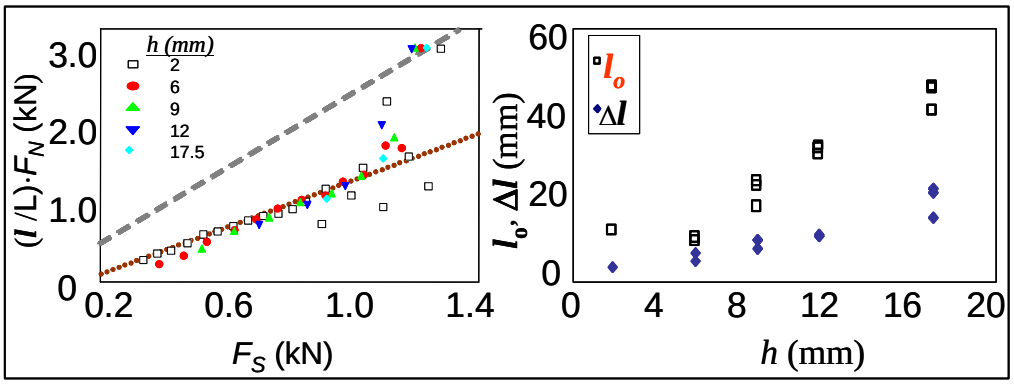

Figure 3: Scaling behaviour of the lengths *l* of successive slip events. **a,** $l/L \cdot F_N$ as a function of F_S, where F_S was applied at different heights, *h*, above the interface. *h* does not influence the $l \propto L \cdot F_S/F_N$ scaling [*Rubinstein et al.*, 2007] (dotted line). Here, F_N = 3*kN* and L=140*mm*. This scaling breaks down at the transition to large events leading to stick-slip motion, described by the Amontons-Coulomb law (dashed line). **b,** The values of both the initial slip length, l_0 (squares), and the incremental extension of each slip event, Δl (diamonds), increase linearly with *h*. l_0 saturates at low *h* suggesting that a minimal length is needed for development of instability. Different points at the same *h* correspond to different F_N.

3.2 *Contact area and fault strength*

We now consider the evolution of the contact area $A(x,t)$. Prior to the first event, $A(x,t)$ is spatially uniform. The passage of each successive precursory slip event (Figure 4) significantly alters the contact area, and hence changes the local fault strength. With each successive event, the

contact area increases in a region of width *D*, that is adjacent to the sample's trailing edge. This process *dynamically* forms an asperity (a localized area whose resistance to slip is much greater

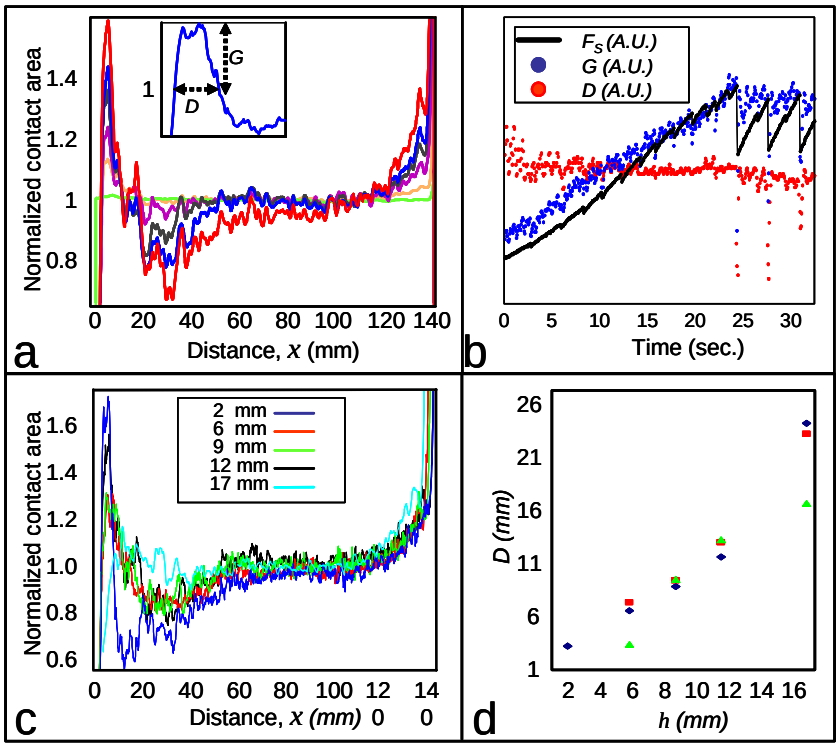

Figure 4: Evolution of the true contact area profile. **a,** *A(x,t)* profiles formed by slip events of increasing length during a single experiment. Deformations of the initially uniform contact profile are both amplified and extended with each slip. (Inset) Close-up of *A(x,t)* profile adjacent to the trailing edge depicting the width *D* and strength *G* of the asperity that is spontaneously formed there. **b**, F_S, *D* and *G* as a function of time for the experiment shown in (a) F_S, *D* and *G* are in arbitrary units to facilitate comparison. The asperity width *D*, stays nearly constant while *G* increases monotonically with F_S. **c,** *D* is determined *h; A(x,t)* in experiments where *h* was varied. The profiles are qualitatively similar in appearance. **d,** *D*, increases nearly linearly with *h*. All profiles in (**c**) were obtained for F_S at 75% of the value needed for the onset of stick-slip. *A(x,t)* in **a** and **c,** is normalized with respect to its spatially uniform value, *A(x, t = 0)*, at the start of the experiment.

than its surroundings [*Lay et al.*, 1982]). Although this asperity continuously strengthens with F_S (Figure 4b), its size, *D*, remains nearly constant throughout each experiment. After overcoming this asperity, each slip both extends the length of the reduced contact area region created by its predecessors, and further reduces *A(x,t)* by a significant amount. This systematic decrease of *A(x,t)* creates a highly weakened region in the asperity's wake. The contact profile, established as a result of this process, is highly non-uniform by the time large-scale overall motion (stick-slip) occurs. As shown in Figure 4c, changes in *h* do not qualitatively affect the general shape of the contact area profiles. Quantitative analysis reveals, however (Figure 4d), that the size of *D* is proportional to *h*.

One may suspect that the variations of the contact area is due to the torque imposed by the F_S, as F_S is applied at a finite height *h* rather than at *h*=0. We found that this effect is negligible over the range of used *h*. For example, the torque resulting from *h*=2mm yields only a 3% variation of the normal stress over the interface length, whereas *A(x,t)* varies by over 50% (Figure 4)

Surprisingly, once a contact profile is created, it is retained by the system, remaining nearly unchanged both after large-scale slip and in successive stick-slip events [*Rubinstein et al.*, 2007]. Large internal stresses are, therefore, also retained by the system, even after major slip events occur. As the contact area mirrors the normal stress values, the existence of this non-uniform profile also indicates that the normal stresses along the interface (or fault) are highly

non-uniform. In particular, the normal stresses along significant regions of the interface are considerably weaker than the remotely applied values would imply.

3.3 *Synthesis of experimental results*

These experiments suggest an intuitive picture for the sequence of events leading to frictional sliding. Before the onset of slip, the loading at the trailing edge imposes a high shear stress region near the edge, whose magnitude decays over a length proportional to h. When F_S is sufficiently large, this highly stressed region yields and an initial crack-like slip event is generated. The slip traverses this region and arrests at a distance, l_0, where the shear stress level is below the slipping threshold. This event results in: (1) slip within the region l_0, where built-up shear stresses are released, (2) elastic deformation of the slider to compensate for the slip-induced contraction in the x direction. The deformation results in an outwardly protruding region of size $D \sim 1/3l_0$ in which the contact area increases, thereby dynamically forming an asperity (cf. Figure 4b). The inwardly bowed region over the remainder of the region l_0, reduces the normal force (=decrease of $A(x,t)$) (3) establishment of a high residual shear stress concentration entrained in the vicinity of the point of arrest of the slip event (This is due to the stress singularity that occurs at the tip of a shear crack.). Upon further increase of F_S, the barrier imposed by the asperity is again overcome and a new slip event is generated. This slip event will easily traverse the weakened region beyond the asperity. Arriving at the tip of the previously arrested event, the new slip event will add sufficient energy to release the energy stored within the high-stress region imposed previously, thereby enabling it to extend itself by Δl. This extension is accompanied by further elastic deformation of the block, thereby increasing the non-uniformity of $A(x,t)$. In this way, each slip event transfers the shear stress imposed at the boundary further along the interface.

4 DISCUSSION

The influence of fault complexity on the dynamics of rupture propagation and seismicity has been the subject of intensive past and recent research [*Aki*, 1979; *Das*, 2003; *Lay et al.*, 1982]. Our experiments suggest that the fingerprint of an 'edge' can be traced, not only to the dynamics of a given rupture, but throughout the entire seismic cycle of a given fault. The results suggest that a geometrical inhomogeneity introduces a scale that may govern the nucleation, size and repeatability of earthquakes along a given fault.

The experiment paints an interesting picture of earthquake dynamics along faults that are loaded asymmetrically (e.g. at an edge or step). They indicate that stress transfer along such faults may be mediated by a periodic sequence of precursory events. This sequence of slip events culminates by the triggering of slowly propagating front, which leads to system size events. The experiments suggest that the early slip events of the periodic sequence (within the scaling regime shown in Figure 3a) "feel" an effectively infinitely long (unsegmented) fault. In contrast, the accelerated growth of l that marks the break of scaling prior to the onset of large events indicates that the dynamics are affected by the fault size during the nucleation phase [*Ohnaka and Shen*, 1999] of a large event. This accelerated increase in l is strongly suggestive of the accelerated seismic release that precedes some large earthquakes [*Bufe and Varnes*, 1993]. The results also imply that precursory sequences of events that initiate from a fault edge strongly modify the fault contact plane prior to a large event.

An excellent example of such slip sequences along a fault edge in the crust is portrayed by the foreshock sequence of the 1998 Sendai Bay event, along the Nagamachi-Rifu fault, Japan [*Umino et al.*, 2002]. In this field case, the main shock of M 5.0 was preceded by 17 foreshocks ranging in magnitude from 1.7 to 3.8 with essentially identical seismic characteristics. The foreshocks sequence lasted about three days with the largest foreshock occurring six minutes prior to the main shock. Mechanical modelling of this sequence of events suggests that the fault was edge-loaded by non-seismic slip in the lower crust [*Nakajima et al.*, 2006]. Accordingly, the foreshock hypocenters propagated upward along the locked part of the Nagamachi-Rifu fault. Finally, Umino et al noted that "A small ambiguous phase…is observed in seismograms of both the M5.0 main shock and the M3.8 largest foreshock…"[*Umino et al.*, 2002]. This slow, low

amplitude ambiguous phase is lacking in the other foreshocks and all aftershocks, and is likely the equivalent of the slow fronts observed in our experiments immediately *before* the main slip event (Fig. 2a). These slow fronts may be akin to the accelerated creep events that are anticipated to be part of the nucleation phase of major earthquakes [*Dieterich and Kilgore*, 1996; *Ohnaka and Shen*, 1999]. Thus, in spite of scale and complexity differences, we note the following similarities between the 1998 Sendai Bay events and our experiments: (1) qualitatively similar (edge) loading conditions, (2) a distinct sequence of precursory events; (3) initiation of precursory events from nearly the same location and (4) a slow ("ambiguous") phase that occurs only before the main event.

In conclusion, these experiments have shown that the fact that shear is applied non-uniformly to a sliding system leads to complex, *systematic* behaviour that appears analogous to natural phenomena, whose source is currently not well understood. We believe that the analogies between our experimental results and seismic observations stem from their similar edge-loading configurations. As elements of edge-loading are common in faults at many scales[*Sagy et al.*, 2007; *Stein et al.*, 1997], it is therefore anticipated that this loading will generate stress distributions that are similar to the laboratory model, and, consequently, may lead to similar dynamics.

5 ACKNOWLEDGMENTS

The authors acknowledge the support of the Israel Science Foundation Grant No. 57/07, grant no. 2006288 awarded by the U.S.-Israel Binational Science Foundation, as well as NSF Continental Dynamics grant No. 0409605 (NELSAM). We also thank E. Brodsky, E. Aharonov, A Sagy, and R. Madariaga for their helpful remarks.

6 REFERENCES

Aagaard, B.T., and T.H. Heaton, Near-source ground motions from simulations of sustained intersonic and supersonic fault ruptures, *Bulletin of the Seismological Society of America*, *94* (6), 2064-2078, 2004.

Aki, K., Characterization of Barriers on an Earthquake Fault, *Journal of Geophysical Research*, *84* (NB11), 6140-6148, 1979.

Ben-Zion, Y., and C.G. Sammis, Characterization of fault zones, *Pure and Applied Geophysics*, *160* (3-4), 677-715, 2003.

Bufe, C.G., and D.J. Varnes, Predictive Modeling of the Seismic Cycle of the Greater San-Francisco Bay-Region, *Journal of Geophysical Research-Solid Earth*, *98* (B6), 9871-9883, 1993.

Das, S., Spontaneous complex earthquake rupture propagation, *Pure and Applied Geophysics*, *160* (3-4), 579-602, 2003.

Dieterich, J.H., and B. Kilgore, Implications of fault constitutive properties for earthquake prediction, *Proceedings of the National Academy of Sciences of the United States of America*, *93* (9), 3787-3794, 1996.

Dieterich, J.H., and B.D. Kilgore, Direct Observation of Frictional Contacts - New Insights for State-Dependent Properties, *Pure and Applied Geophysics*, *143* (1-3), 283-302, 1994.

Harris, R.A., and S.M. Day, Dynamics of Fault Interaction - Parallel Strike-Slip Faults, *Journal of Geophysical Research-Solid Earth*, *98* (B3), 4461-4472, 1993.

Johnson, A.M., R.W. Fleming, and K.M. Cruikshank, Shear Zones Formed Along Long, Straight Traces of Fault Zones During the 28 June 1992 Landers, California, Earthquake, *Bulletin of the Seismological Society of America*, *84* (3), 499-510, 1994.

Lachenbruch, A.H., and J.H. Sass, Heat-Flow and Energetics of the San-Andreas Fault Zone, *Journal of Geophysical Research*, *85* (NB11), 6185-6222, 1980.

Lapusta, N., and J.R. Rice, Nucleation and early seismic propagation of small and large events in a crustal earthquake model, *Journal of Geophysical Research-Solid Earth*, *108* (B4), 2205, 2003.

Lay, T., H. Kanamori, and L. Ruff, The Asperity Model and the Nature of Large Subduction Zone Earthquakes, *Earthquake Prediction Research*, *1* (1), 3-71, 1982.

Matsuura, M., and T. Sato, Loading mechanism and scaling relations of large interplate earthquakes, *Tectonophysics*, *277* (1-3), 189-198, 1997.

Nakajima, J., A. Hasegawa, S. Horiuchi, K. Yoshirnoto, T. Yoshide, and N. Umino, Crustal heterogeneity around the Nagamachi-Rifu fault, northeastern Japan, as inferred from travel-time tomography, *Earth Planets and Space*, *58* (7), 843-853, 2006.

Ohnaka, M., and L.F. Shen, Scaling of the shear rupture process from nucleation to dynamic propagation: Implications of geometric irregularity of the rupturing surfaces, *Journal of Geophysical Research-Solid Earth*, *104* (B1), 817-844, 1999.

Reches, Z., G. Schubert, and C. Anderson, Modeling of Periodic Great Earthquakes on the San-Andreas Fault - Effects of Nonlinear Crustal Theology, *Journal of Geophysical Research-Solid Earth*, *99* (B11), 21983-22000, 1994.

Rice, J.R., and Y. Ben-Zion, Slip complexity in earthquake fault models, *Proceedings of the National Academy of Sciences of the United States of America*, *93* (9), 3811-3818, 1996.

Rubinstein, S.M., G. Cohen, and J. Fineberg, Detachment fronts and the onset of dynamic friction, *Nature*, *430* (7003), 1005-1009, 2004.

Rubinstein, S.M., G. Cohen, and J. Fineberg, Dynamics of precursors to frictional sliding, *Physical Review Letters*, *98* (22), 2007.

Rubinstein, S.M., M. Shay, G. Cohen, and J. Fineberg, Crack like processes governing the onset of frictional slip, *Int. J. of Fracture*, *140*, 201-212, 2006.

Sagy, A., E.E. Brodsky, and G.J. Axen, Evolution of fault-surface roughness with slip, *Geology*, *35* (3), 283-286, 2007.

Shaw, B.E., and J.H. Dieterich, Probabilities for jumping fault segment stepovers, *Geophysical Research Letters*, *34* (1), 2007.

Stein, R.S., A.A. Barka, and J.H. Dieterich, Progressive failure on the North Anatolian fault since 1939 by earthquake stress triggering, *Geophysical Journal International*, *128* (3), 594-604, 1997.

Umino, N., T. Okada, and A. Hasegawa, Foreshock and aftershock sequence of the 1998 M 5.0 Sendai, northeastern Japan, earthquake and its implications for earthquake nucleation, *Bulletin of the Seismological Society of America*, *92* (6), 2465-2477, 2002.

Wesnousky, S.G., Predicting the endpoints of earthquake ruptures, *Nature*, *444* (7117), 358-360, 2006.